Mapping the Dense Molecular Gas in the Strongest Star-forming Galaxies

Abstract

We propose an EAO Legacy Survey to construct the largest and deepest HCN J=4→3 and HCO^+ J=4→3 (the strongest collisionally excited molecular lines after CO) maps in a complete infrared (IR) flux limited sample of 23 brightest IR galaxies. Previous ~ 100 hrs observations with the IRAM 30m lead to a large HCN J=1→0 map in M 51, demonstrating the large-scale extended distribution of dense molecular gas beyond the nuclear ~ kpc regions in spiral galaxies. The HARP-B array on the JCMT provides the unique mapping machinery in studying the dense gas excitation, chemistry, probing even denser and warmer gas at close to the peak ladder in the spectral line energy distribution in these molecular lines. This survey will help shed fundamental new light on how the molecular gas forms stars on different physical scales and under various physical environments. The survey will offer a unique database, via diagnostic power of various line ratios (HCN, HCO^+ & CO), for connecting the emissions between dense molecular gas tracers and star formation (SF) in both central cores of galaxies and more extended regions in spiral disks. Combining with our ongoing efforts with the JCMT and other telescopes and the rich data in literature, this survey will also raise the opportunity to tackle many scientific issues including the initial conditions of SF, chemistry, kinematics, feedbacks of SF and AGN, excitation conditions of molecules, as well as the connections between SF and dense molecular gas on various physical scales. We select the sample from the IRAS Revised Bright Galaxy survey with $f_{60\mu m} > 50$ Jy and $f_{100\mu m} > 100$ Jy. We plan to map HCN J=4→3 and HCO^+ J=4→3 along the major axes of 16 nearby galaxies and fully sample the 2′×2′central inner disk regions of 7 galaxies with the largest sizes. The planed observations will reach to a sensitivity of 0.3 K km s^{-1} (~4.5×10^6 $M_\odot$) per beam, with a linear resolution from 0.2 to 2.8 kpc. The survey sample consists of 23 nearest and brightest infrared galaxies beyond the local group that already have extremely abundant legacy data from ground to space and needs a modest ~270 hrs band 3 time (some portions can be observed under weather bands 2 and 4 and they are also estimated for each) to complete. This will be **the first systematic dense gas mapping survey in the off-central regions of nearby galaxies**.

List of co-Is

Name	Affiliation	Country	Name	Affiliation	Country
Kotaro Kohno	U. Tokyo	JP	Stephen Serjeant	Open U.	UK
Masa Imanishi	NAOJ	JP	Jeff Wagg	SKA Org.	UK
Daisuke Iono	NAOJ	JP	Christine Wilson	McMaster U.	CA
Quang Nguyen Luong	NAOJ	JP	Erik Rosolowsky	U. Alberta	CA
Y.-P. Ao	NAOJ	JP	J.-Z. Wang	SHAO	CN
Satoki Matsushita	ASIAA	TW	L. Cheng	SHAO	CN
Aeree Chung	Yonsei U.	KR	T. Xiao	SHAO	CN
Sungeun Kim	Sejong U.	KR	J.-W. Wu	NAOC	CN
Yujin Yang	KASI	KR	Matt Smith	Cardiff U.	UK
Padelis Papadopoulos	Cardiff U.	UK	Q.-S. Gu	NJU	CN
Walter Gear	Cardiff U.	UK	Y. Shi	NJU	CN
Haley Gomez	Cardiff U.	UK	H. Chen	NJU	CN
Serena Viti	UCL	UK	J.-F. Wang	XMU	CN
George Kelly	UCL	UK	Y.-H. Zhao	PMO	CN
Amelie Saintonge	UCL	UK	X.-J. Jiang	PMO	CN
Richard Tunnard	UCL	UK	Q.-H. Tan	PMO	CN
Elias Brinks	U. Hertfordshire	UK	L.-J. Liu	PMO	CN
Mark Sargent	U. Sussex	UK	C.-T. Yang	PMO	CN
Dimitra Rigopoulou	U. Oxford	UK	D.-Z. Liu	PMO	CN
			T.-T. Fang	XMU	CN

Co-PIs: Yu Gao (PMO, CN), Zhiyu Zhang (U. Edinburgh, UK), Thomas Greve (UCL, UK)

1 Background and Motivation:

1.1 Dense Molecular Gas — Key to Star Formation

The star formation (SF) process constantly turns gas into stars and is what drives galaxy formation. It is, however, not yet fully understood how the gas properties affect the ability to form stars. Questions which naturally arise are: Which phases of gas are directly connected to SF, what kind of physical processes regulate SF and its feedback, and is there a universal physical law applying for all types of SF and all kinds of galaxies near and far?

Based on observations of CO and HI, which trace molecular (H_2) and atomic gas respectively, the Kennicutt-Schmidt (K-S) law relates the global surface-densities of SF rate (Σ_{SFR}) and total amount of neutral gas (Σgas :HI+ H_2) in star-forming galaxies by introducing a super linear exponent, $\alpha \sim 1.4$ ($\Sigma_{SFR} \propto \Sigma_{gas}^{\alpha}$) (Kennicutt & Evans 2012). This empirical relationship connects total gas and SF, but the super linear α indicates a non-constant SF efficiency increases with different SF rate, traced by infrared (IR) luminosity L_{IR}. Quite a range of deviation from the K-S law, however, has also been found in different types of galaxy samples, both in global and in spatially resolved studies with (sub)kpc resolutions (e.g., Kennicutt & Evans 2012; Bigiel et al. 2008).

With high spatial resolution and large scale mapping observations of ^{12}COJ=2→1 and HI in nearby normal spiral galaxies, it is found that HI is not related to SF (e.g., Bigiel et al. 2008). For the H_2 gas traced by low-J ($J \leq 2$) CO emission, SF is nearly linearly correlated with H_2, in the disks of local spiral galaxies even to the extended HI dominated outer disk regions (e.g., Bigiel et al. 2008; Schruba et al. 2011; Leroy et al. 2013). This linearity, however, only holds in a very narrow range of surface density of SF and on physical scales greater than 200 pc. Moreover, this relation becomes super linear when starburst regions and extreme starbursts such as ultraluminous IR galaxies (ULIRGs) are included (e.g., Genzel et al. 2010; Daddi et al. 2010).

The dense molecular gas ($n(H_2) \geq 10^4 cm^{-3}$) stands out to have much tighter and direct connection with SF than that of total gas (HI+ H_2) or only H_2. Gao & Solomon (2004a,b, see Fig. 1) have shown that galaxies exhibit a linear correlation between the far-IR and HCN J=1→0 luminosities, over three orders of magnitude range. These correlations even extend dense cores in giant molecular clouds (GMCs) in the Milky Way (Wu et al. 2005; Zhang et al. 2014a). These results imply that the dense gas is the gas phase that is forming stars. The change of the slopes of the K-S relation in different galaxy samples simply reflects the variation of the dense gas fraction (e.g., Lada et al. 2010).

Recent advances in our understanding of SF do suggest that active high-mass SF, is *essentially and exclusively* formed in the dense cores of GMC (e.g., Evans 2008). The dense gas tracers (e.g., HCN, HCO^+, CS etc.) exhibit, beside CO, the strongest collisional excited lines in galaxies (e.g., Riechers et al. 2006; Graciá-Carpio et al. 2008; Baan et al. 2008; Greve et al. 2014), suggesting that the extremely high SF efficiency found in ULIRGs simply reflects the tremendous amount of *dense* molecular gas available, but not the total gas mass content(e.g., Lada et al. 2010). More IR luminous galaxies tend to have higher SF rate per unit total molecular mass, whereas the SF rate per unit dense molecular mass is likely constant (Gao & Solomon 2004a,b).

Liu et al. (2015b) have examined the relations between the galaxy averaged surface densities of the various gas components (atomic, molecular, total gas, and dense molecular gas) and SF rate in a sample of 181 local galaxies with IR luminosities spanning ~ five orders of magnitude. We have taken a novel approach and used high-resolution radio continuum observations to measure accurately the sizes of the areas of active SF within the galaxies, a key step as it directly affects the surface densities of gas and SF. In our sample, we find that the surface density of dense molecular gas (as traced by HCN) has the tightest correlation with that of SF rates, and is linear in log–log space (power-law slope of N = 1.01 ± 0.02) across the full galaxy sample (see Fig. 2). The correlation between surface densities of molecular gas (traced by CO) and Σ_{SFR} is sensitive to the adopted value of the CO-to-H_2 conversion factor used to infer molecular gas masses from CO luminosities. If instead we adopt conversion factor values of 4.6 and 0.8 for disk galaxies and (U)LIRGs, respectively, we find the two galaxy populations separate into two distinct Σ_{SFR} versus Σ_{H2} relations. We find no correlation between global surface densities of SF rates and atomic gas.

1.2 General Properties of High Density Gas Tracers

The low-J transitions ($J \leq 2$) of CO lines have critical densities of only $\sim$ 300 - 1000 cm^{-3} /τ [1], making them good tracers of the mass of total H_2 gas (M_{H_2}). This density range matches well with the bulk of the GMCs. However, the bulk of molecular gas is not forming stars everywhere. Only the gas at high density in the dense cores has sufficiently high density to collapse and eventually form stars. A physical connection between the H_2 gas density and SF is actually expected, as this is where gravity dominates the turbulent pressure in the clouds, leading to collapse and fragmentation and eventual formation of stars.

By climbing up the n_{crit} of molecular gas tracers, we can gain insight into the physics from the bulk of the molecular gas to the sites of on-going SF, and further explore how the gas density affects SF process. The rotational transitions of the molecules with high dipole moments and high abundances by number compared to that of hydrogen ($\sim 10^{-6} - 10^{-8}$ relative to H_2; e.g., HCN, HCO^+, CS, etc.), become the most common tracers of dense gas since they are the most luminous molecular lines after CO and even observable in high redshift. Detailed studies of HCN and HCO^+in bright, nearby galaxies can then be useful and much needed in extending our knowledge in the local Universe to help interpret observations in galaxies at high redshift.. The J=1–0 transition of these molecules have a n_{crit} of $10^4 - 10^6$cm^{-3} , which are representative H_2 density of Galactic dense cores (e.g., Plume et al. 1997; Wu et al. 2005).

For the J=1–0, 3–2, and 4–3 transitions of HCN, n_{crit} are $\sim 2 \times 10^5$ cm^{-3} , 5×10^6 cm^{-3} , and 1.5×10^7 cm^{-3} , and upper level energies are 4 K, 26 K, and 46 K, respectively. The high-J transitions are also less affected by the line trapping, so the effective n_{crit} keeps uninfluenced from column density. So, the high-J transitions probe **very high density and relatively warm** cores which are heated up by the star formation. High-J ($J \geq 5$) CO transitions, also have high n_{crit}. However, the high-J CO lines also need very high kinetic temperature ~hundreds of K to be excited efficiently. The high-J CO transitions are also difficult to access from the ground while the HCN and $HCO^+$are readily available.

1.3 Chemical Properties of High Density Gas Tracers

Through comparison with models, abundances of molecules tracing dense gas and their line ratios can be used not only to infer the physical conditions of the gas but also to constrain the chemical reactions that drive molecule formation and destruction in irradiated regions(e.g., van Dishoeck & Blake 1998). Subject to a proper interpretation, observations of molecular emission are extremely sensitive to trace the material that is the reservoir or leftover of the star formation process, as well as the process of star formation itself. Molecular abundances can be interpreted through models for Photon-Dominated Regions (PDRs), X-ray Dominated Regions (XDRs), Mechanical Dominated Regions (MDRs), and are among the best diagnostics for disentangling star formation.

In general and on large scales, the overall abundance of molecules is determined by the density of the gas, which favours their formation. and the energetic processes, such as UV or X-ray radiation, which in general tend to destroy molecules. The abundances of different molecules vary in different physical environments, such as super wind from starbursts, strong radiation from AGNs, jets and outflows, large scale shocks in merging activities, Cosmic Rays, etc. Specifically, chemical processes between HCN, HNC, and CN could change their abundances in different temperatures (Baan et al. 2008). The ratios between HCN and HCO^+ could also be affected by chemical complexities(e.g., Krips et al. 2008), ionization rates and electron densities (e.g. Papadopoulos 2007), and shocks (e.g., Xie et al. 1995). All above issues make it difficult to find a stable dense gas tracer in the extreme environment of galaxies.

The use of molecules as diagnostics of different gas conditions stems from the fact that different molecules *and* different transitions of the same molecule will trace different regions of a galaxy from the cold, relatively low density molecular gas (mostly traced by CO), to highly shocked regions, traced by e.g., SiO, and finally to very high density star forming clouds (traced by e.g., HCN). Often high abundances of particular species such as HCO^+ are automatically attributed to the presence of strong PDRs, since this molecule is indeed abundant in the presence of a strong UV field, regardless of the metallicity, cosmic ray ionisation rate or density of the galaxy (e.g., Bayet et al. 2011). Nevertheless this species is also highly enhanced when the cosmic ray or

[1]For multiple energy level molecular system: $n_{crit} = \Sigma_{l<u} A_{ul} / \Sigma_{l \neq u} C_{ul}$, or a given T_{kin} (Jansen 1995; Osterbrock & Ferland 2006).

X-ray ionisation rates are high, regardless of the UV field (e.g., Bayet et al. 2011; Meijerink & Spaans 2005; Meijerink et al. 2007).

This apparent degeneracy is common to most molecules and again reflects the fact that chemistry is a non linear process influenced by a combination of energetics and physical conditions. Although there is no unique single molecular transition can linearly translate the line flux to the mass of star forming gas in these complex glaxies, a proper use of theoretical models coupled with the acquision of **line ratios between several different molecules (e.g., HCN, HCO^+, and CO)** will help us to determine and quantify the dense gas in star forming galaxies.

2 Previous and Ongoing Work

2.1 Galactic and Extragalactic Studies on Dense Gas and SF

Considerable work has been done on the relationship between dense gas and SF in both Galactic and extragalactic studies, especially for the HCN, HCO^+, and CS lines. With the observations of HCN J=1→0 toward 65 galaxies, Gao & Solomon (2004a,b) found a strong linear correlation (N = 1) between HCN and IR luminosities. As shown in Fig. 1 this relation has been extended to the Milky Way dense cores (Wu et al. 2005) and possibly to high-z galaxies and QSOs as well (Gao et al. 2007). With both total IR luminosity and 1.4 GHz radio continuum as SFR tracers and the size tracer of SF, Liu et al. (2015b) compiled the largest sample (181 galaxies) of HCN J=1→0 found that $\sigma_{\rm HCN}$ and $\sigma_{\rm SFR}$ are linearly correlated globally.

As well as HCN, many other molecular transitions have been widely studied for such correlations, both in Galactic dense cores and in external galaxies. Baan et al. (2008) carried out a survey of HCN, HNC, and CN in nearby active SF galaxies, and found variation of $L_{\rm IR}$-$L'_{\rm line}$ in different molecules. Graciá-Carpio et al. (2008), and García-Burillo et al. (2012) performed a new HCN J=1→0 survey with IRAM 30m, and argue that HCN J=1→0 likely have either a bimodal or super-linear correlation with $L_{\rm IR}$, because the excitation of HCN J=1→0 could be enhanced by IR pumping at 14 μm (Weiß et al. 2007; Sakamoto et al. 2010). Wang et al. (2011) performed a CS J=5→4 survey in nearby SF galaxies, where they found linear correlation between $L_{\rm IR}$ and $L'_{\rm CS\,J=5-4}$. Mao et al. (2010) and Wilson et al. (2012) show that ^{12}COJ=3→2 has a linear correlation with $L_{\rm IR}$ globally, and for the nearby galaxies without complete ^{12}COJ=3→2 maps, the correlations are sub-linear.

Bussmann et al. (2008) observed HCN J=3→2 in a subsample of Gao & Solomon (2004a), and found a $L_{\rm IR}$-$L'_{\rm HCN\,J=3-2}$ index less than unity (0.72 ± 0.08). Juneau et al. (2009) compiled data of ^{12}COJ=1→0, HCO^+ J=1→0, HCO^+ J=3→2, HCN J=1→0, and HCN J=3→2. They found sub-linear slope indices too. Most of these results, however, are highly under debate, because they correlate the dense gas measured in small beamsizes with IR emission from the whole galaxies, so their slopes of correlations are likely under-estimated.

The linear correlations between SF and dense gas are also found in Galactic dense cores, which expand the luminosity range to up to eight orders of magnitudes, and naturally connect to galaxies. Wu et al. (2010) mapped HCN J=1→0 and J=3→2, and CS(J=2→1) and J=7→6 in Galactic massive star-forming cores. All these dense gas tracers show linear correlations with both virial mass and IR emission. Reiter et al. (2011) use CS(J=2→1) , CS J=7→6, HCN J=1→0, HCN J=3→2, HCO^+, N_2H^+, HNC, C_2H etc. to study the luminosity correlations between $L_{\rm IR}$ and $L'_{\rm gas}$ in Galactic dense cores, and find correlations for all these lines. Ma et al. (2013) studied HCO^+ J=1→0 in ~ 300 Galactic clumps, and also found a linear correlation between $L_{\rm IR}$ and $L'_{\rm gas}$. So, the linearity of these correlations could be explained as a "fundamental unit" of SF in different physical scales, thus the SFR and the mass of dense gas can be simply piled up by adding in more star-forming units (Wu et al. 2005).

The recent advance of the *Herschel* Space Observatory has produced a large mid-to-high-J CO database in various types of local galaxies and Galactic sources. Liu et al. (2015a) analyzed nine mid-to-high-J CO (J=4→3 to 12→11) transitions in a largest sample of 167 local galaxies including spatially resolved mapping data, so as to probe the dense and warm molecular gas properties. They found that all the nine CO transitions are linearly and tightly correlated with the FIR luminosities which have been matched to the beamsize of each CO line. They further demonstrated that the linearities and tightness are valid from high-z "normal" star-forming BzKs all the way down to Galactic young stellar objects (YSOs)/protostars over *14 orders of magnitude*. **All these results indicate that the physics of SF in dense gas is universally invariant across the cosmic time**

and physical scales.

Given the large uncertainties in $L_{\rm IR}$ for a large fraction of SMGs compared to BzKs (from SED fitting), the amount of excess in FIR/COJ=5→4 (i.e. dense gas star formation efficiency) in SMGs should still be treated with caution. And this excess is not significant enough to break down a linear form of dense gas versus SF relation, as these starbursts are the most extreme systems at all redshifts and as such do not represent the dominant mode of SF observed in main sequence (MS) galaxies (e.g. BzKs). Thus, better FIR measurements e.g. via SEDs, and observations of other dense gas tracer in local normal MS galaxies are needed before making solid conclusions at high-z, as a benchmark.

2.2 Challenges between Theoretical and Observational Results

On the other hand, theories on dense gas and star formation are largely under debate and few of them match observational results. Krumholz & Thompson (2007) propose that SF is controlled by the free fall time scale as: $\dot{M}_* = SFR_{\rm ff} M_{\rm gas}/t_{\rm ff}(\overline{n})$, where $t_{\rm ff}(\overline{n})$ is the free-fall time, and $SFR_{\rm ff}$ is a number of order 10^{-2}. This result, however, is not consistent with the observational results in multiple transition CS studies (i.e., Zhang et al. 2014a), who found that **the free-fall time scale does not play a role in the dense gas phase.**

Based on the non-local thermodynamic equilibrium (non-LTE) radiative transfer calculations, Narayanan et al. (2008) performed hydrodynamic simulations of disk and merging galaxies, and quantitatively reproduced the observed $L_{\rm IR}$-$L'_{\rm gas}$ relations for HCN J=1→0 and CO J=1→0. Follow up predictions show that the slope indices of $L_{\rm IR}$-$L'_{\rm gas}$ decreases with $n_{\rm crit}$ or J-transitions of the molecular lines. They argue that the correlations is controlled with the fraction of thermalized molecular gas at a given molecular transition, and their models predict that the slope indices of $L_{\rm IR}$-$L'_{\rm gas}$ decrease with $A_{\rm ul}/\Gamma_{\rm ul}$ or the J-transitions of gas tracers, because the gas tracers with $A_{\rm ul}/\Gamma_{\rm ul} > A_{\rm ul}/\Gamma_{\rm ul}({\rm HCN\ J\ =\ 1\ -\ 0}) \sim 10^6 {\rm cm}^{-3}$ are sub-thermally excited (e.g., Krumholz & Thompson 2007; Narayanan et al. 2008; Juneau et al. 2009). Their simulations, however, lack enough spatial resolution to resolve the dense change in SF cores thus are obliged to adopt sub-gridding physics. Using CS J=7→6, HCN J=4→3, and HCO$^+$ J=4→3, Zhang et al. (2014a) find that *irrespective of the $n_{\rm crit}$ of a specific transition, dense molecular gas is universally related in a linear way to star forming activities for self-gravitationally bound gas systems.*

Lada et al. (2012) argue that the linear correlations between dense gas and SF is purely controlled by the fraction of dense gas contained within the clouds or galaxies, and propose that there is a threshold of SF volume density, beyond which clouds will inevitably collapse by gravity. By star counting and $A_{\rm V}$-deduced column density in 20 Galactic GMCs (c2d and COMPLETE surveys), Heiderman et al. (2010) found SF threshold to be $\sim 130 M_\odot/{\rm pc}^{-2}$. Such methods, however, can not extend to extragalactic studies.

Most of the observations in galaxies discussed above, however, were performed in the central nuclear region, while the more SF quiescent and colder outer disks have relatively weaker emission and lower surface brightness. The off-nuclear regions still remain difficult to study. Usero et al. (2015) observed HCN J=1→0 in several off-nuclear positions of nearby galaxies, and they found, surprisingly, that the dense gas on disks has higher SF efficiencies than the linear correlations found in galaxies globally. This result opens a new question: **Does the star formation in the low surface density regions (disks) have different mode than that in the high surface density regions (nuclear regions), and if yes, what physical conditions take control of it?** More observational data with different physical conditions in galaxies are urgently needed to test and verify theoretical studies.

2.3 Ongoing Efforts on Dense Gas with Various Telescopes, and ALMA Highlights

In the past few years we have made series of systematic surveys of dense gas tracers in nearby SF galaxies. Using GBT 100m, IRAM 30m, APEX 12m, SMT 10m, we performed a series of surveys of multiple transition lines of CS (J=1→0, 2→1, 3→2, 5→4, and 7→6), HCN J=1→0, HCN J=4→3, and HCO$^+$ J=4→3 in nearby star-forming galaxies, including normal spiral galaxies, starbursts, and ULIRGs. These transitions cover a $n_{\rm crit}$ range of $10^4 - 10^7 {\rm cm}^{-3}$.

These results, however, are still largely limited in active star-forming galaxies, or the centres of SF galaxies, where the $\Sigma_{\rm SFR}$ is high. For the low-$\Sigma_{\rm SFR}$ regime, few HCN maps of external galaxies are available (e.g., Nguyen

et al. 1992; Gao & Solomon 2004a; Kepley et al. 2014), simply because the HCN emission in normal spiral disks is weak. Till now, little is known about the dense gas distribution outside the central regions in external galaxies.

We have performed a pilot survey of dense gas emission along the major axis of a few spiral galaxies, for HCN J=1→0 in M 51. Fig. 4 shows the HCN J=1→0 emission distributes over large scale in spiral galaxies. The extent of dense gas traced by HCN J=1→0 is as large as the *Herschel* 70 μm image which traces SF activities. When we plot the luminosities of HCN J=1→0 and IR in Fig. 5, we find that the best fitting of the $L_{\rm IR}$-$L'_{\rm HCN\,J=1-0}$ slope index become sub-linear to ~0.74, for all measured data points. However, if we limit the data to be only from the disk region, the slope for the $L_{\rm IR}$-$L'_{\rm HCN\,J=1-0}$ correlation is about unity ~ 1.06 (Chen et al. 2015). This indicates that the dense gas SFE in the central regions is likely higher than that in the outer disk region by an factor of two. This finding seems to be consistent with (Usero et al. 2015), that is, the SF processes on the disks may have a different mode than that in the central region of galaxies.

There are also other possibilities need to be tested. The calculation of dense gas mass may not follow the same conversion $X_{\rm HCN}$ factor in different physical conditions. The AGN in the nuclear region could also play a role in exciting the HCN J=1→0 emission, and contribute to the total IR luminosity. So, more detailed studies are needed to confirm the findings, and to exploit the underlying physics. A dedicated calibration of dense gas mass tracer in different physical environments (e.g., $T_{\rm kin}$, $n(H_2)$, radiation fields, etc.) is urgently needed in the disks of nearby galaxies.

With the unprecedented sensitivity of ALMA, high resolution observations with dense gas tracers (HCN, HCO^+, CS, etc.) in nearby SF galaxies are possible. These studies mostly focus on local (U)LIRGs, and the line ratios between HCN, HCO^+, and CS are likely largely influenced by AGN activities (e.g., Izumi et al. 2013; Martín et al. 2015; García-Burillo et al. 2014; Imanishi & Nakanishi 2014) and SF activities (e.g., Meier et al. 2015). In many cases, the starburst-type galaxies show very large molecular line widths and high HCN J=4→3-to-HCO^+ J=4→3 flux ratios, which indicate that turbulence-induced heating may also play a role in enhancing the HCN emission. The HCN J=4→3-to-HCO^+ J=4→3 line ratios could be used to detect more energetic activity than normal starbursts, including deeply buried AGNs, in dusty galaxy populations(e.g., Imanishi & Nakanishi 2014).

3 Science Goals:

3.1 HCN J=4→3 and HCO^+ J=4→3 Mapping in Nearby Galaxies

Although there exist over a hundred nearby galaxies have HCN measurements, few have ever been mapped and none is mapped extensively beyond the central ~kpc. The spatially-resolved observations of HCN J=1→0 emission in the nearby spiral galaxy M 51 using the IRAM 30 m telescope covers an extent of $4' \times 5'$ with spatial resolution of $28''$, which is, so far, the largest in M 51(i.e., Chen et al. 2015). There is a correlation between infrared emission (SF rate indicator) and HCN J=1→0 emission (dense gas tracer) at kpc scale in M 51, a natural extension of the proportionality between the SFR and the dense gas mass established globally in galaxies. The IR-HCN correlations in M 51 are further compared with the global ones from Milky Way to high-z galaxies and bridge the gap between giant molecular clouds (GMCs) and galaxies. Like the centers of nearby galaxies, the IR/HCN ratio measured in M 51 (particularly in the central regions), is slightly lower than what is measured globally in galaxies, yet is still within the scatter. This implies that though the IR/HCN ratio varies as a function of physical environment in the different positions of M 51, IR and HCN indeed show a linear correlation over 10 orders of magnitude.

Although some HCN/HCO^+ 4→3 observations were obtained in ~ 20 galaxies (Zhang et al. 2014a), few mapping exists in any galaxies yet except for example, the small maps in M82 (Seaquist & Frayer 2000a) and NGC 253 (Knudsen et al. 2007). However, it is still not possible to connect the extragalactic and Galactic results due to a gap in the correlation plot between GMC and galaxy scales. It also does not seem possible to detect dense gas emission in nearby dwarf galaxies (mostly metal poor) or Low Surface Brightness Galaxies (it is even hard for CO (e.g., Shi et al. 2015; Matthews & Gao 2001), let alone other molecular lines). HCN mapping (e.g., mapping along the galaxy major axes) in nearest and strongest galaxies, could however offer the hope to fill the gap in these correlations spanning over 10 orders of magnitude, when appropriate spatial

resolution corresponding to certain scales is selected. Nevertheless, until now, the dense gas emission in nearby galaxies has been mostly observed in the central nuclear regions only, except for a few off-nuclear positions (e.g., Bayet et al. 2009; Usero et al. 2015).

We aim to: 1) verify the GLOBAL SF law for nearby galaxies, 2) compare the dense gas properties of the disks with those in central regions, 3) study the local resolved SF law of HCN using $L_{\rm IR}$, $L'_{\rm HCN\,J=4-3}$, and HCO$^+$ J=4→3 at every single pointing across the spiral disks.

As an example, Fig. 3 shows CS J=2→1 mapped along the major axis of Maffei 2, where strong lines were detected far out of the central nuclear region. From our 45 hour pilot project JCMT (M15BI112) for mapping HCN J=3→2 along the major axes of a few nearby IR-bright galaxies in the 15B semester. Fig. 6 shows our recently obtained spectra on the disks of these galaxies, which successfully detected emission from off-center regions.

Observations along the major axes and fully sampled the central nuclear region in galaxies will also give us the distribution of the dense gas from nuclear centers to outer parts in the inner disks, and help to answer following questions: How much dense gas is distributed beyond the nuclear starburst regions (typically of 1′) in star-forming galaxies? How does the HCN J=4→3 and HCO$^+$ J=4→3 emission differ from HCN/HCO$^+$ J=1→0, and how does the ratio of HCN/HCO$^+$(J=4→1)/(J=1→0) change along the major axes? How do the dense gas emission lines change as compared to CO?

3.2 Synergy with *Herschel* FTS high-J CO and Modeling

The *Herschel* space observatory has provided a treasure of the CO spectral line energy distribution (SLED), with the complete CO SLED from the J = 5→4 to 13→12 transitions, and the [CII] 158 μm and [O I] 63 and 146 μm lines (covered by PACS). Such observations have been done not only for the ULIRGs (e.g, The *Herschel* Comprehensive Emission Survey (HerCULES, open time key program, PI: van der Werf), but also in the less luminous LIRGs (*Herschel* Spectroscopy Survey of Warm Molecular Gas in Local Luminous Infrared Galaxies, PI: Nanyao Lu), and nearby normal spiral galaxies (e.g., Beyond the Peak Survey, PI: JD. Smith) as well.

For the LIRGs and ULIRGs, the CO SLED (i.e., line flux vs. J) typically rises up to the J=5→4 to J=7→6 transitions and subsequently decreases for higher J-levels. It is a key finding for these galaxies, however, that the CO lines remain remarkably excited – on the global scale – all the way up to J=13→12. In fact, the high-J CO lines (J > 7) typically dominates the total CO luminosity of (U)LIRGs, constituting as much as 60% of the total (e.g., Greve et al. 2014; Kamenetzky et al. 2014). While there is broad agreement that the observed CO SLEDs require a multi-phased ISM, what powers the hot gas responsible for the strong high-J CO lines is a highly contested issue. On the basis that samples of LIRGs and less luminous sources exhibit a linear (i.e., slope of unity) IR vs. CO luminosity relation up to very high transitions (J=13→12) it has been argued that the high-J emission must emerge from dense PDR regions where the primary power source is UV photons from nearby O and B stars (e.g., Liu et al. 2015a). A significant subset of the most luminous (U)LIRGs, however, have such extreme global high-J vs. low-J CO line ratios (easily exceeding that of the Orion complex) that if they were powered by UV light from stars it would imply vastly higher dust temperatures (> 100 K) than what is observed(∼ 40 K e.g., Greve et al. 2014). In these cases the likely culprit is strong mechanical feedback from either supernovae- or merger-driven shocks.

From the CO lines only, however, it is very difficult to derive the real physical conditions, because of the degeneracy of $T_{\rm kin}$, $n(H_2)$, abundance with dv/dr. A simple two components LVG modeling, often push the temperature to be extremely high (> 1000 − −5000 K; e.g., Schirm et al. 2014), or, extraordinary low (barely above the CMB temperature; e.g., Glenn et al. 2015), which are both unphysical. Combining with multiple molecules, especially the dense gas tracers like HCN, HCO$^+$, and CS, it is possible to break the degeneracy, by decomposing gas excitation with at least two components. A prime example hereof is NGC 6240, show extreme high-J CO lines that is coming from a hot and highly turbulent gas phase residing between the two starburst nuclei, i.e., far away from stellar UV light (e.g., Papadopoulos et al. 2014; Tunnard et al. 2015). With the rich CO SLEDs in Herschel archive, and heating/cooling analysis, the HCN and HCO$^+$ lines are the key to solve the power source of high-J CO lines. Moreover, the CO SLED peaks at J ∼7 on the disks (FTS results; e.g., Lu et al. 2014, 2015; Liu et al. 2015a), while HCN and HCO$^+$ mostly peak at J=4, to be revealed by the

proposed survey.

3.3 Characterizing the Physical Conditions and Excitations of the SF Units Probed by HCN/HCO$^+$

The J =4→-3 lines of HCN and HCO$^+$ are especially valuable as in almost all galaxies they lie on the high−J side of the Spectral Line Energy Distribution (SLED), so that when combined with the J=1→0 lines (which have been observed, at least in HCN, in all of our targets) these lines place tight constraints on the physical conditions in the observed galaxies (e.g., Papadopoulos et al. 2014). In sources where the J=3→2 line has also been observed the SLED can be fitted extremely well.

Combined with the HCO$^+$ observations and CO data from the literature the observations will be analysed with non-LTE radiative transfer models. We have developed a series of radiative transfer codes (e.g., Zhang et al. 2014b; Tunnard et al. 2015) to analyze molecular excitation conditions with Bayesian probability distribution using large velocity gradient (LVG) approach. These state-of-the-art tools could decompose the observed SLEDs into multi-phase LVG components. Furthermore, the degeneracies between $T_{\rm kin}$, $n(H_2)$, and dv/dr could be broken by combining multiple molecules as well as by modelling the chemistry under different physical and chemical conditions and compare the derived abundance and line profiles with the observations. Our team has in house chemical, shock and radiative transfer models (Viti et al. 2011, Rawlings & Yates 2001), in addition to in house 1- and 3-D PDR codes (Bisbas et al. 2014). We will be able to run a large grid of models, some including shocks, and complete a statistical analysis comparing observations in different regions to simulations. These allow a systematic study on the physical conditions in a statistically meaningful sample of galaxies.

With the planned survey in HCN/HCO$^+$ as well as low-J observational data, it allows us to study the gas mass - line luminosity conversion factors for different molecules in a wide range of physical parameter space and different galactic environments. These conversion factors are invaluable for high redshift studies of galaxies, where the required integration time frequently restricts observations to a single line. The HCN, CS and HCO$^+$ conversion factors are likely to be far more useful for identifying the mass of star-forming gas phase (and thereby, combined with FIR measurements of the SFR and SFE) than CO does (e.g., Zhang et al. 2014a).

The mapping observations with sufficiently spatial resolution and extent will be uniquely suited to the JCMT with HARP, and they will allow us to map the distribution of HCN J=4→3, revealing excitation gradients and kinematics across the inner disks of these spiral galaxies. Comparing these new lines with archival optical, IR and CO observations will allow us to study in detail the relationships between SF, diffuse molecular gas and dense molecular gas across the central regions of these galaxies. As well as being valuable in their own right, these observations will contribute to the expanding corpus of extragalactic molecular line observations and as such will be an extremely valuable literature resource.

4 Sample Selection and Technical Justification

4.1 Sample Selection and Mapping Plans

With the multi-pixel receiver HARP, the large collecting area of JCMT, and the low water vapor condition at Manua Kea in Hawaii, we plan to carry out mapping observations of HCN J=4→3 and HCO$^+$ J=4→3 toward the nearest/brightness galaxies beyond the local group. We select a sample of 22 nearby galaxies from the IRAS Revised Bright Galaxy Sample (RBGS, i.e. Sanders et al. 2003). All galaxies that are JCMT-visible ($\delta > -40^\circ$) with $f_{60\mu m} > 50$ Jy and $f_{100\mu m} > 100$ Jy have been included in our sample (except M31 and M33 that are extremely large in size). The infrared flux density cutoffs are specifically used in order to select all nearby star-forming galaxies with the capability of detecting dense gas emission over large spatial scale beyond the nuclear starburst regions. All galaxies in our sample have been detected in HCN J=1→0 emission, and most of HCN J=1→0 data are from Gao & Solomon (2004a). Table 1 presents the list of the selected targets with HCN J=1→0 detections, IR flux density, distance, and source size. The IR luminosity ranges from $2.5\times10^9 L_\odot$ (Maffei 2) to $3.2\times10^{11} L_\odot$ (Arp299).

For the most extended galaxies (e.g., IC 342, NGC 253, etc.), we plan to perform a fully sampled map within the central $\sim 2' \times 2'$ region. These galaxies are mostly face-on, and the SF is mostly concentrated in

the central regions. The H_2 gas/dust emission drops exponentially with increasing radius(Leroy et al. 2009), making their gas suburbs extremely difficult to be detected. For the rest of the galaxies, we plan to perform mapping observations along the major axes where the surface densities of SFR and H_2 gas are relatively higher than that of face-on galaxies (the dense gas will be effectively in a very thin layer in the equatorial plane of the galaxies, however, the dense gas under an inclination might not lead to seeing multiple dense gas clumps along the line of sight through the disk). In the latter case, even if we can not get a fully sampled map, the emission along the major axes would be sufficient for characterizing radial distributions of physical parameters. At least four pixels of the receiver array can cover the major axes simultaneously.

4.2 Technical Justification

We propose to map 23 nearby galaxies in HCN J=4→3 and HCO^+ J=4→3 emission. The observing frequency ranges from 350.89 GHz to 356.75 GHz and the HARP receiver is employed. For the 6 galaxies with $D \gtrsim 10'$ and strongest HCN J=1→0 line peak intensity, we plan to fully sample the nuclear regions of galaxies with a jiggle mapping mode (3×3 pattern, 10″ beam spacing), while the rest of galaxies are selected to be mapped along the major axes using grid mode (see Fig. 7 for a sketch of the observing mode). A wobbler switching mode will be employed to guarantee flat baselines. For a few nearby galaxies with large sizes (e.g., IC 342, NGC 5457), we will use position switching mode to avoid possible weak emission from the reference position.

4.3 Observing Time Estimate

We estimate the HCN J=4→3 line peak intensity based on the observed HCN J=1→0 flux by assuming a brightness temperature ratio of HCN J=4→3 to HCN J=1→0 of r_{41}=0.12, which is an average value measured from the nearby spirals that have been detected in both HCN J=1→0 and HCN J=4→3 (Gao & Solomon 2004a; Zhang et al. 2014a, note that the beam size of HCN J=1-0 observations is generally larger than HCN J=4-3 and thus here we might underestimate the value of r_{41}). We also note that the value r_{41}=0.12 we adopted is more than two times smaller than the value measured for local (U)LIRGs ($r_{41} \geq 0.27$, see Papadopoulos 2007). For a conservative time estimate, we think adopting a smaller value of r_{41} might be suitable since we plan to mapping dense gas emission in the galaxies.

For the largest galaxies that are planned to be fully sampled in the nuclear region, we assume the T_{peak} of outermost position is 1/5-1/10 of the central T_{peak}, while for the galaxies mapped along the major axes, the T_{peak} of outermost position is 2/3-1/5 of the central T_{peak}, with two or three pointing per galaxy. On average the observations need to reach a rms noise level of 1.5 mK (T^*_A) in order to achieve an S/N≥3 detection at the outermost positions. We have used HITEC to estimate integration time by assuming a band 3 weather condition with τ_{225GHz}=0.1 and a spectral resolution of 25 km/s (see Fig. 8 for the sample of HiTEC GUI set up). The total observing time required for HCN J=4→3 mapping survey in 23 targets is 135 hours (see Table 1 for the detailed time estimate of each target). We also calculate the observing time by assuming weather condition of band 2 and band 4 (see Table 1), respectively. For the strongest targets with T_{peak}(HCN J=4→3)> 80 mk (e.g., NGC 253, Maffei 2, NGC 1068, IC342), the observations can be carried out under band 4 weather condition with a reasonable integration time (t_{obs} ~ 4.5–7 hours for one target). For the weakest sources in our sample, a better weather condition (e.g., band 2) would certainly save observing time, but under average band 3 weather, the observations can also be done with slightly longer time. Assuming the HCO^+ J=4→3 emission is as strong as HCN J=4→3 (see Zhang et al. 2014a), we will roughly need a same amount of time for HCO^+ J=4→3 mapping observations. Thus, **the total observing time we request for our dense gas mapping survey program is 270 hours**.

5 Management, Observations, Data Release, and Publication

The project is led by a coordinating team of members including the coordinator (Yu Gao), Co-PIs, and regional representatives. The current list of Co-Is is presented on the cover page. The team consists of experts with rich observational experiences in radio astronomy. The observations and data reduction will be effectively implemented. The consortium will ensure the qualities of **scientific direction, observational runs, data reduction,**

publications, and data release.

5.1 Membership Policy

Astronomers from all the JCMT partner institutes are welcome to join before the submission of the proposal. After the proposal is accepted, new partners or international participations need recommendation from the coordinating team and the EAO board.

The survey is designed for a few major science topics but it does not limit science directions. All members are highly encouraged to use the data for their scientific researches. Participation of other members are welcome and constructive comments are the minimum requirement for being in the author list of any paper. Internal collaboration and follow-up surveys with other telescopes are encouraged. A reasonable effort will be made to avoid conflict projects and to protect graduate student projects.

5.2 Observing and Data Archiving Management

We aim to finish about seven sources per year during the survey period, so that the analysis and publication can start right after the first data arrival. At the beginning of each semester, we will organize series telecons to discuss the observational progress and the priority of targets.

The data reduction will be performed on the JCMT pipeline first and will be optimised using our own pipeline, to ensure the quality of the data. Standing waves, bad channels, and irrecoverable baselines are expected to be removed semi-automatically following standard procedures. We therefore anticipate to perform data quality assurance (QA) checks in several stages, including QA-0 (raw), QA-1 (sensitivity, $T_{\rm sys}$ check), QA-2 (optimised cubes after removing all bad data). We will release the QA-0 and QA-2 data to public on the project website. The consortium is responsible for establishing a high-quality dataset and the data will be released a full year following completion of the semester in which the data was taken.

A website will be set up at either EAO or PMO for the public data release and presentation. We will provide primary products such as spectral line cubes, moments maps, as well as science products such as ratio maps between HCO^+, HCN, and CO. These data will benefit both Galactic and extragalactic communities, and will also serve as a pathfinder for follow-up ALMA surveys.

5.3 Publication Management

As soon as the proposal is accepted, we will prepare the first paper describing the samples. In the first year (semester 16A & 16B) of the project, we will concentrate on developing the methodology to cover the main science goals observed during the preceding semester. The initial papers should describe the analysis methods of the main science goals to the first set of observed targets.

During the second (17A & 17B) and third (18A & 18B) years, we will extend our analysis to other targets and perform follow-up observations. There are several Ph.D. dissertation work in the team are tightly related to this survey too. We will produce publications in several aspects utilizing also previous JCMT archival observations (both molecular line and continuum) in ULIRGs and Galactic targets, as compared to active SF arms and starburst regions etc. Several members in the team are working on theoretical works including simulation, chemistry, and molecular excitation modellings. Subsequent scientific analysis and theoretical interpretation will be addressed. Our team also has expertise on the fields of IR, X-ray, optical wavelengths, etc. so that we will have detailed studies on multi-band comparison with IR radiation field, X-ray intensity and their ratios over a variety of scales and physical environments. Major scientific output and the survey publications will be presented on the project website.

References

Baan, W. A., Henkel, C., Loenen, A. F., Baudry, A., & Wiklind, T. 2008, A&A, 477, 747

Bayet, E., Aladro, R., Martín, S., Viti, S., & Martín-Pintado, J. 2009, ApJ, 707, 126

Bayet, E., Williams, D. A., Hartquist, T. W., & Viti, S. 2011, MNRAS, 414, 1583

Bigiel, F., Leroy, A., Walter, F., et al. 2008, AJ, 136, 2846

Bussmann, R. S., Narayanan, D., Shirley, Y. L., et al. 2008, ApJ, 681, L73

Chen, H., Gao, Y., Braine, J., , & Gu, Q. 2015, ArXiv:1507.08506

Daddi, E., Elbaz, D., Walter, F., et al. 2010, ApJ, 714, L118

Evans, II, N. J. 2008, in Astronomical Society of the Pacific Con-

ference Series, Vol. 390, Pathways Through an Eclectic Universe, ed. J. H. Knapen, T. J. Mahoney, & A. Vazdekis, 52
Gao, Y., Carilli, C. L., Solomon, P. M., & Vanden Bout, P. A. 2007, ApJ, 660, L93
Gao, Y. & Solomon, P. M. 2004a, ApJS, 152, 63
Gao, Y. & Solomon, P. M. 2004b, ApJ, 606, 271
García-Burillo, S., Combes, F., Usero, A., et al. 2014, A&A, 567, A125
García-Burillo, S., Usero, A., Alonso-Herrero, A., et al. 2012, A&A, 539, A8
Genzel, R., Tacconi, L. J., Gracia-Carpio, J., et al. 2010, MNRAS, 407, 2091
Glenn, J., Rangwala, N., Maloney, P. R., & Kamenetzky, J. R. 2015, ApJ, 800, 105
Graciá-Carpio, J., García-Burillo, S., Planesas, P., Fuente, A., & Usero, A. 2008, A&A, 479, 703
Greve, T. R., Leonidaki, I., Xilouris, E. M., et al. 2014, ApJ, 794, 142
Heiderman, A., Evans, II, N. J., Allen, L. E., Huard, T., & Heyer, M. 2010, ApJ, 723, 1019
Imanishi, M. & Nakanishi, K. 2014, AJ, 148, 9
Izumi, T., Kohno, K., Martín, S., et al. 2013, PASJ, 65, 100
Jansen, D. J. 1995, PhD thesis, Leiden Observatory, Leiden University, P.O. Box 9513, 2300 RA Leiden, The Netherlands
Juneau, S., Narayanan, D. T., Moustakas, J., et al. 2009, ApJ, 707, 1217
Kamenetzky, J., Rangwala, N., Glenn, J., Maloney, P. R., & Conley, A. 2014, ApJ, 795, 174
Kennicutt, R. C. & Evans, N. J. 2012, ARA&A, 50, 531
Kepley, A. A., Leroy, A. K., Frayer, D., et al. 2014, ApJ, 780, L13
Knudsen, K. K., Walter, F., Weiss, A., et al. 2007, ApJ, 666, 156
Kohno, K., Ishizuki, S., Matsushita, S., Vila-Vilaró, B., & Kawabe, R. 2003, PASJ, 55, L1
Krips, M., Neri, R., García-Burillo, S., et al. 2008, ApJ, 677, 262
Krumholz, M. R. & Thompson, T. A. 2007, ApJ, 669, 289
Lada, C. J., Forbrich, J., Lombardi, M., & Alves, J. F. 2012, ApJ, 745, 190
Lada, C. J., Lombardi, M., & Alves, J. F. 2010, ApJ, 724, 687
Leroy, A. K., Walter, F., Bigiel, F., et al. 2009, AJ, 137, 4670
Leroy, A. K., Walter, F., Sandstrom, K., et al. 2013, AJ, 146, 19
Liu, D., Gao, Y., Isaak, K., et al. 2015a, ArXiv:1504.05897
Liu, L., Gao, Y., & Greve, T. R. 2015b, ApJ, 805, 31
Lu, N., Zhao, Y., Xu, C. K., et al. 2014, ApJ, 787, L23
Lu, N., Zhao, Y., Xu, C. K., et al. 2015, ApJ, 802, L11
Ma, B., Tan, J. C., & Barnes, P. J. 2013, ApJ, 779, 79
Mao, R.-Q., Schulz, A., Henkel, C., et al. 2010, ApJ, 724, 1336
Martín, S., Kohno, K., Izumi, T., et al. 2015, A&A, 573, A116
Matthews, L. D. & Gao, Y. 2001, ApJ, 549, L191
Meier, D. S., Walter, F., Bolatto, A. D., et al. 2015, ApJ, 801, 63
Meijerink, R. & Spaans, M. 2005, A&A, 436, 397
Meijerink, R., Spaans, M., & Israel, F. P. 2007, A&A, 461, 793
Narayanan, D., Cox, T. J., Shirley, Y., et al. 2008, ApJ, 684, 996
Nguyen, Q.-R., Jackson, J. M., Henkel, C., Truong, B., & Mauersberger, R. 1992, ApJ, 399, 521
Osterbrock, D. E. & Ferland, G. J. 2006, Astrophysics of gaseous nebulae and active galactic nuclei
Papadopoulos, P. P. 2007, ApJ, 656, 792
Papadopoulos, P. P., Zhang, Z.-Y., Xilouris, E. M., et al. 2014, ApJ, 788, 153
Plume, R., Jaffe, D. T., Evans, II, N. J., Martin-Pintado, J., & Gomez-Gonzalez, J. 1997, ApJ, 476, 730
Reiter, M., Shirley, Y. L., Wu, J., et al. 2011, ApJS, 195, 1
Riechers, D. A., Walter, F., Carilli, C. L., et al. 2006, ApJ, 645, L13
Sakamoto, K., Aalto, S., Evans, A. S., Wiedner, M. C., & Wilner, D. J. 2010, ApJ, 725, L228
Sanders, D. B., Mazzarella, J. M., Kim, D.-C., Surace, J. A., & Soifer, B. T. 2003, AJ, 126, 1607
Schirm, M. R. P., Wilson, C. D., Parkin, T. J., et al. 2014, ApJ, 781, 101
Schruba, A., Leroy, A. K., Walter, F., et al. 2011, AJ, 142, 37
Seaquist, E. R. & Frayer, D. T. 2000a, ApJ, 540, 765
Seaquist, E. R. & Frayer, D. T. 2000b, ApJ, 540, 765
Shi, Y., Wang, J., Zhang, Z.-Y., et al. 2015, ApJ, 804, L11
Tunnard, R., Greve, T. R., Garcia-Burillo, S., et al. 2015, ArXiv:1507.07565
Usero, A., Leroy, A. K., Walter, F., et al. 2015, ArXiv:1506.00703
van Dishoeck, E. F. & Blake, G. a. 1998, Annual review of astronomy and astrophysics, 36, 317
Wang, J., Zhang, Z., & Shi, Y. 2011, MNRAS, 416, L21
Weiß, A., Downes, D., Neri, R., et al. 2007, A&A, 467, 955
Wilson, C. D., Warren, B. E., Israel, F. P., et al. 2012, MNRAS, 424, 3050
Wu, J., Evans, II, N. J., Gao, Y., et al. 2005, ApJ, 635, L173
Wu, J., Evans, II, N. J., Shirley, Y. L., & Knez, C. 2010, ApJS, 188, 313
Xie, T., Allen, M., & Langer, W. D. 1995, ApJ, 440, 674
Zhang, Z.-Y., Gao, Y., Henkel, C., et al. 2014a, ApJ, 784, L31
Zhang, Z.-Y., Henkel, C., Gao, Y., et al. 2014b, A&A, 568, A122

Table 1: Sample of galaxies to be mapped in HCN(4-3) and HCO^+(4-3)

N	Source Name	R.A.	Decl.	Distance	Diameter	$f_{60\mu m}$	$f_{100\mu m}$	$\log L_{\rm fir}$	$\log\Sigma_{SFR}$	$T_{\rm peak}^{\rm (HCN10)}$	$T_{\rm peak}^{\rm (HCN43)}$	$T_{\rm disk}^{\rm (HCN43)}$	$t_{\rm obs-band3}^{\rm (HCN43)}$	$t_{\rm obs-band2(4)}^{\rm (HCN43)}$
		(J2000)	(J2000)	(Mpc)	(arcmin)	(Jy)	(Jy)	($L_\odot$)	($M_\odot {\rm yr}^{-1}{\rm kpc}^{-2}$)	(mK)	(mk)	(mk)	(hrs)	band-2(4)(hrs)
(1)	(2)	(3)	(4)	(5)	(6)	(7)	(8)	(9)	(10)	(11)	(12)	(13)	(14)	
1	∗**NGC 253**	00 47 33.1	−25 17 18	2.5	27.5×6.8	967.81	1288.15	10.29	0.05	330	180	18	2	1(4.5)
2	∗NGC 660	01 43 02.4	13 38 42	14.0	8.3×3.2	65.52	114.74	10.38	0.37	4[c]	11	5	5	3(10)
3	∗NGC 891	02 22 33.4	42 20 57	10.0	13.5×2.5	66.46	172.23	10.18	-1.76	16	9	4	7	4(15)
4	Maffei 2	02 41 55.0	59 36 15	2.8	5.82×1.57	135	225	10.00	0.42	150	80	8	3	2(6.5)
5	∗**NGC 1068**[a]	02 42 40.7	−00 00 48	16.7	7.1×6.0	196.37	257.37	10.89	1.92	35[d]	80	10	3.5	2(7)
6	NGC 1097	02 46 19.0	−30 16 30	16.4	9.3×6.3	53.35	104.79	10.59	-0.08	30[e]	8	5	8.5	4.5(22)
7	∗NGC 1365[a]	03 33 36.4	−36 08 25	20.8	11.2×6.2	94.31	165.67	10.86	0.55	10[c]	30	8	5	2.5(15)
8	∗**IC 342**	03 46 48.5	68 05 47	3.7	21.4×20.9	180.80	391.66	10.01	-2	45[c]	135	15	3	1.5(7)
9	NGC 1808[a]	05 07 42.3	−37 30 47	10.5	6.5×3.9	105.55	141.76	10.55	0.61	18[f]	25	8	5	2.5(15)
10	∗NGC 2146	06 18 37.7	78 21 25	15.2	6.0×3.4	146.69	194.05	10.93	0.44	30	16	8	6	3(18)
11	∗NGC 2903	09 32 10.1	21 30 03	6.2	12.6×6.0	60.54	130.43	10.05	-1.22	15	8	4	8	4.5(16.5)
12	∗**M82**[b]	09 55 52.7	69 40 46	3.5	11.2×4.3	1480.42	1373.69	10.61	1.05	100	50	10	7	3.5(18)
13	∗NGC 3079	10 01 57.8	55 40 47	16.2	7.9×1.4	50.67	104.69	10.65	-0.4	6[c]	18	6	5	2.5(10.5)
14	NGC 3521	11 05 48.6	−00 02 09	8.2	11.0×5.1	49.19	121.76	9.84	-1.55	12	6	4	8	5(18)
15	∗NGC 3627	11 20 14.9	12 59 30	8.1	9.1×4.2	66.31	136.56	10.24	-1.43	4[c]	12	5	4.5	3(10)
16	∗NGC 3628	11 20 17.0	13 35 23	9.6	14.8×3.0	54.80	105.76	10.14	-0.85	10[c]	30	5	5	3(10)
17	Arp 299	11 28 30.4	58 34 10	54.1	...	113.05	111.42	11.74	0.3	12	6	4	8.5	5.5(18)
18	∗NGC 4631	12 42 08.0	32 32 29	8.1	15.5×2.7	85.40	160.08	10.10	-1.9	3.5[c]	10	5	5	3(10.5)
19	NGC 4736	12 50 53.0	41 07 14	4.8	11.2×9.1	71.54	120.69	9.59	-1.01	10	5	4	8.5	5(19)
20	M51	13 29 52.7	47 11 43	7.6	11.2×6.9	97.42	221.21	10.31	-1.78	50	27	5	6.5	4(15)
21	∗**M83**	13 37 00.9	−29 51 56	3.7	12.9×11.5	265.84	524.09	9.94	-1.44	23[c]	70	10	6.5	3.5(17)
22	NGC 5457	14 03 12.5	54 20 56	5.2	28.8×26.9	88.04	252.84	10.13	-2.14	10	5	4	9.5	5.5(22)
23	∗**NGC 6946**	20 34 52.3	60 09 14	5.5	11.5×9.8	129.78	290.69	10.01	-1.68	17[c]	50	10	5	2.5(12)

Note. – Galaxy name marked with asterisk (∗) indicates the HCN(1-0) data are from Gao & Solomon (2004a). For the rest of galaxies, the HCN(1-0) data are from Chen et al. (2015) [M51], Baan et al. (2008) [NGC 1808, Arp 299], Usero et al. (2015) [NGC 3521, NGC 4736, NGC 5457], Nguyen et al. (1992) [Maffei 2], and Kohno et al. (2003) [NGC 1097]. Galaxies that are planned to be observed in jiggle mapping mode (3×3 pattern, 10" beam spacing, 12×12 pixels) are marked in boldface, and the others are selected to be mapped along the major axes using grid mode. **Col.(1) & (2)**: source number and name. **Col.(3) & (4)**: source coordinate. **Col.(5)**: source distance. **Col.(6)**: major and minor diameters of galaxies, taken from NED. **Col.(7) & (8)**: IRAS 60μm and 100μm flux density, adopted from Sanders et al. (2003). **Col.(9)**: far-infrared luminosities. **Col.(10)**: SFR surface densities from Liu et al. (2015b). **Col.(11)**: HCN(1-0) line peak intensity, measured by various telescopes. Except the data marked with notes (c,d,e,f), the rest are from IRAM 30m. **Col.(12)**: the expected HCN(4-3) line peak intensity in the central position of each galaxy. To convert the line peak $T_{\rm mb}$ to flux density, we adopt $S/T_{\rm mb}$=5 Jy/K for IRAM 30m, $S/T_{\rm mb}$=28 Jy/K for NRAO 12m, $S/T_{\rm mb}$=22 Jy/K for FCRAO 14m, and $S/T_{\rm mb}$=18 Jy/K for JCMT 15m. **Col.(13)**: the HCN(4-3) line peak intensity in the outermost weakest position that expected to be detected. **Col.(14)**: the total integration time for each galaxy to be mapped in HCN(4-3) under the assumption of band 3 weather condition. **Col.(15)**: the integration time estimated by assuming weather condition of band 2 and band 4 (in parenthesis), respectively.
[a] The peak $T_{\rm mb}$ of HCN(4-3) measured in NGC 1068, NGC 1365, and NGC 1808 with the APEX 12m are about 34 mK, 16 mK, and 15 mK, respectively (Zhang et al. 2014a). [b] The peak $T_{\rm mb}$ of HCN(4-3) measured in the central position of M82 with the JCMT is about 45 mK (Seaquist & Frayer 2000b).
[c] Data from the NRAO 12m. [d] Data from the FCRAO 14m. [e] Data from the NRO 45m. [f] Data from the SEST 15m.

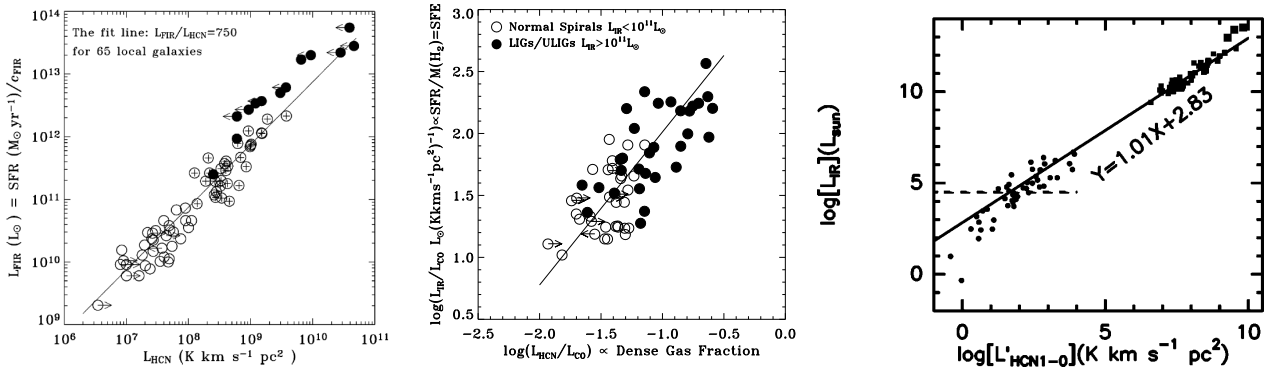

Figure 1: Left: The HCN-FIR correlation (the fit is for local normal galaxies with a slope of 1 (open circles)). Filled circles are high-z AGN/galaxies (Gao et al. 2007) and circles with plus signs are local (U)LIRGs. Middle: The correlation between $L_{\rm HCN}/L_{\rm CO}$ and $L_{\rm IR}/L_{\rm CO}$ for a local sample (Gao & Solomon 2004a). Right: The correlation between $L_{\rm IR}$ and $L_{\rm HCN}$ for Galactic and extragalactic sources (Wu et al. 2005).

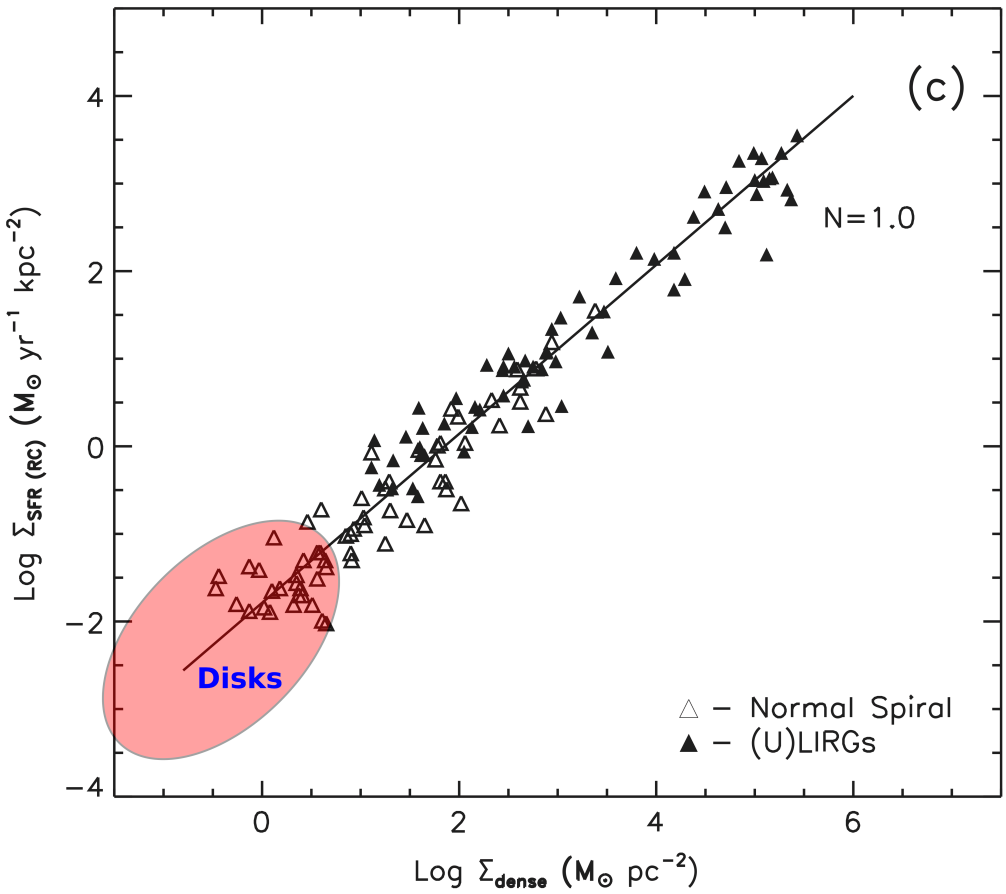

Figure 2: Σ_{dense} as a function of Σ_{SFR}. The Σ_{dense} - Σ_{SFR} relation is the tightest one among all correlations, and it is linear (N=1.01 ± 0.02). Fitting to normal galaxies and (U)LIRGs separately yields identical linear correlation within the uncertainties.

Figure 3: CS J=2→ 1 mapping along the major axis of the Maffei 2 galaxy. The unit of x and y axes are both in arcsec. This map was taken in less than 2 hours observing time with the IRAM 30m.

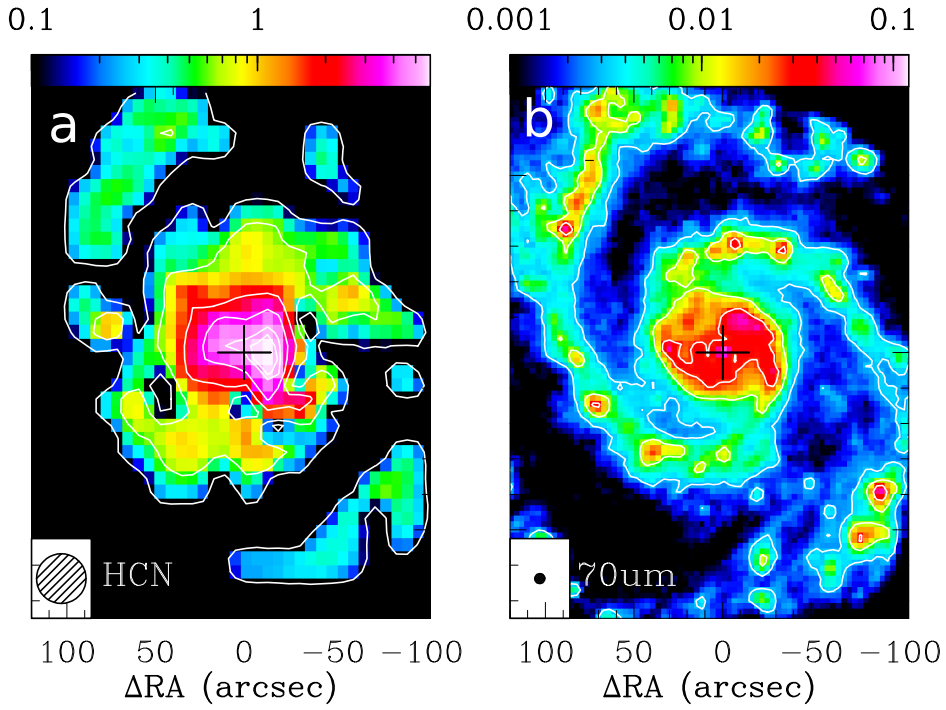

Figure 4: (a) Integrated intensity map of HCN J=1→0 of M 51. Contour levels are : 0.1, 0.6, 1.9, 3.4, 4.9, 5.4 K km s^{-1} (on $T_{\rm mb}$ scale) . (b) *Herschel* 70 μm image with contour levels of 3, 9, 27,81 mJy/pixel. The crosses mark the central position of M 51 with α = 13 : 29 : 52.7, δ = 47 : 11 : 43.0 (J2000).

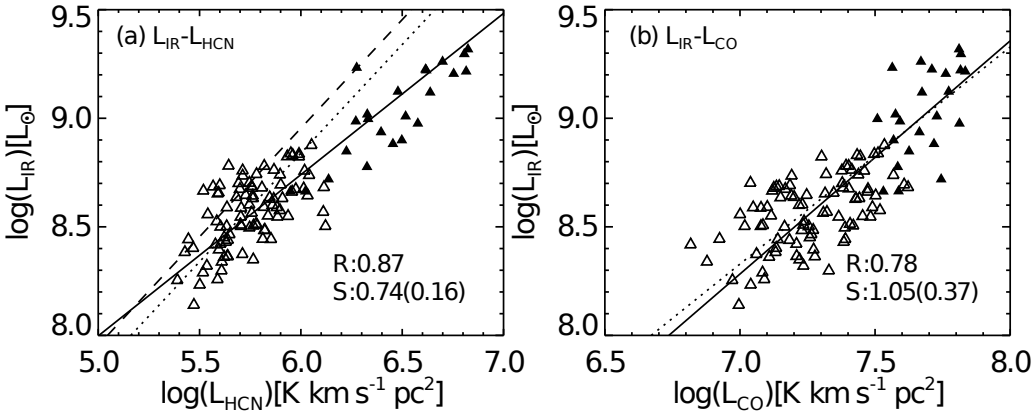

Figure 5: $L_{\rm IR}$ as a function of $L'_{\rm HCN\,J=1-0}$in M 51. Each symbol corresponds to an individual pointing in the observations. The pointings in the central region are marked with filled triangles, and the open triangles show the pointings on the disk. The solid line shows the best fit for all data. The dotted line indicates the fit with the data only on the disk.

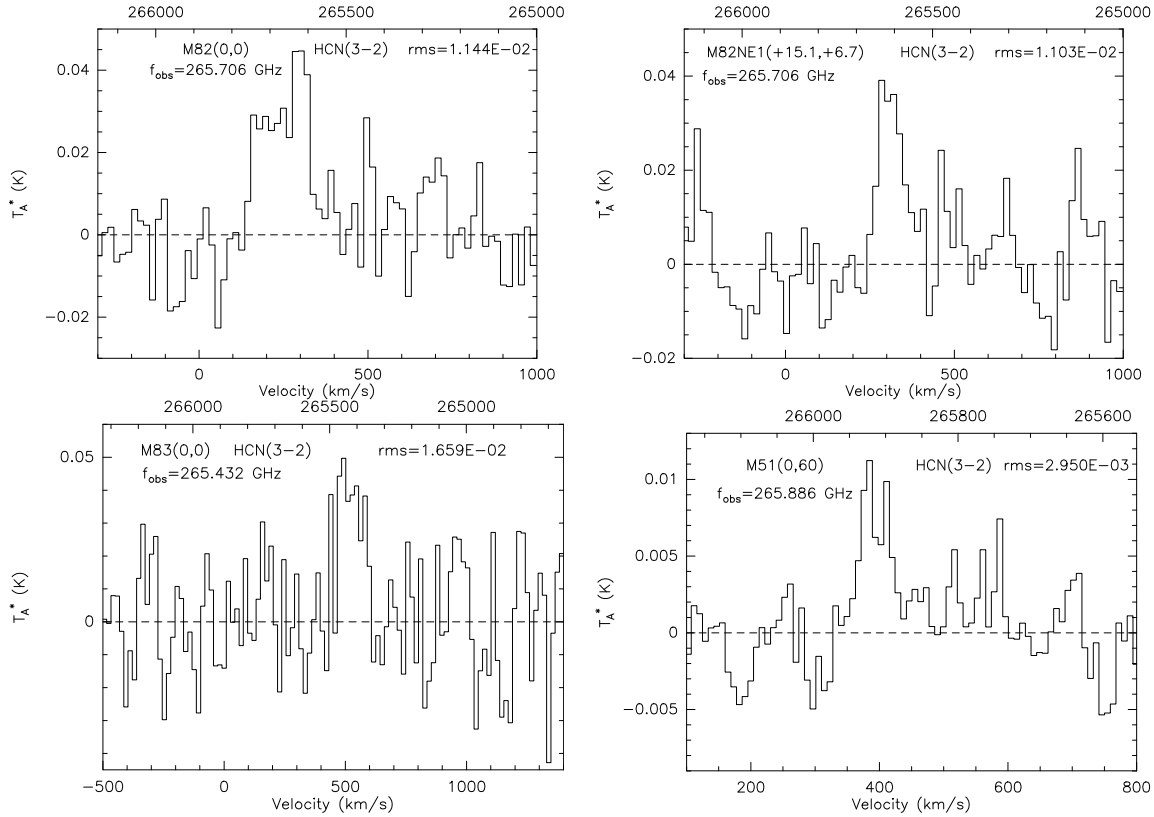

Figure 6: HCN J=3→2 spectra in the central position of M 82 (top left), the northeast off-center position of M 82 (top right), the central position of M 83 (bottom left), and the north off-center position of M 51 (bottom right). The spectra are smoothed to 17 km s^{-1} for display (8.8km s^{-1} for M51). The M 82 spectra are from our 45 hr JCMT Project (M15AI50) aiming to map HCN J=3→2. The spectra of M 51 were taken with CSO which aims to map HCN J=3→2 in the disk region.

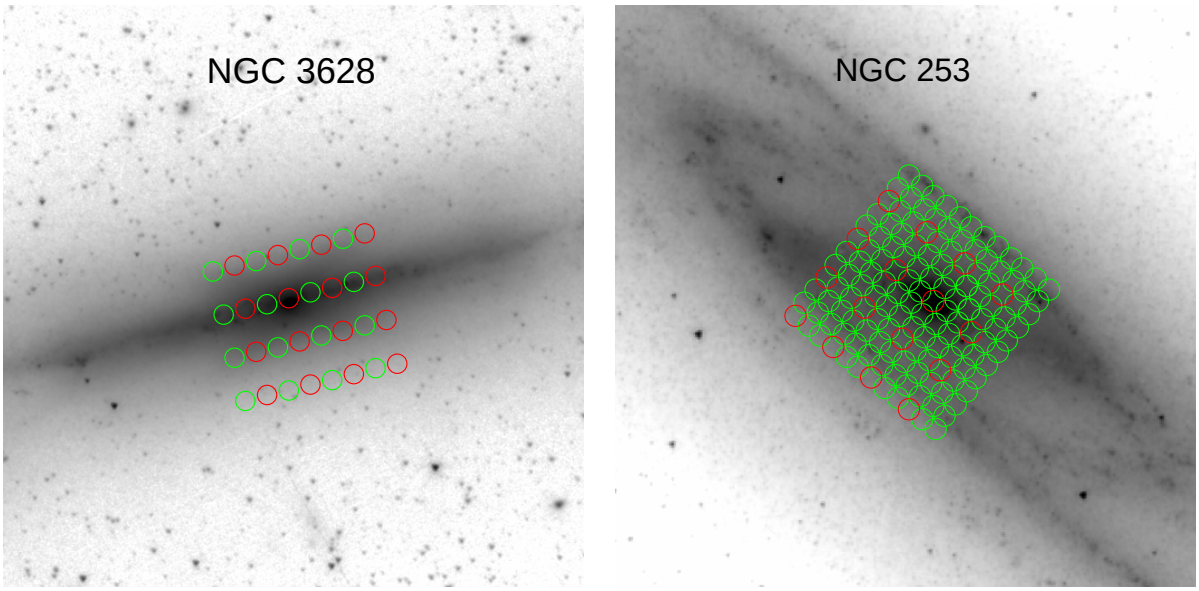

Figure 7: The sample schematic diagrams of a grid mode (**left**) and a jiggle mode (**right**) observations. The beam width is 13″ at 355 GHz and the beam spacing is 15″ for two points grid pattern observation. For the observing mode with 3×3 jiggle pattern that fully sample the nuclear region of extended galaxies (e.g.,NGC253/NGC1068/IC342/M82/M83/NGC6946), the beam spacing is 10″.

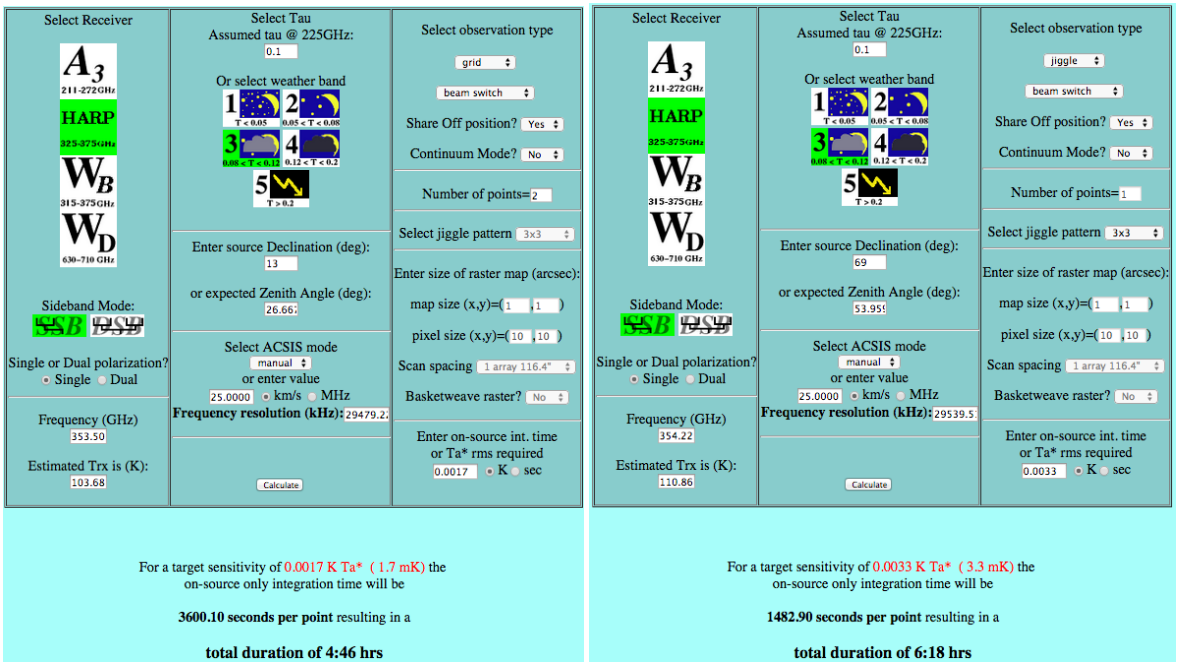

Figure 8: Two sample screen grabs of the HiTEC GUI set up.